Thermal Exchange of Glass Micro-Fibers Measured by the 3ω Technique

Tuyen Duc D Nguyen, Jacques Richard, J. Doumouro, Y. de Wilde, Olivier Bourgeois

Thermal exchange of glass micro-fibers measured by the 3ω technique

T.D. Nguyen
Institut NEEL, Univ. Grenoble Alpes
CNRS-25 avenue des Martyrs
F-38042 Grenoble, France
e-mail: tuyenkstnk46@gmail.com

J. Richard
Institut NEEL, Univ. Grenoble Alpes
CNRS-25 avenue des Martyrs
F-38042 Grenoble, France
e-mail: jacques.richard@neel.cnrs.fr

J. Doumouro
Institut Langevin, ESPCI Paris
Université PSL, CNRS, 1 rue Jussieu,
F-75005, Paris, France
e-mail: joris.doumouro@espci.fr

Y. De Wilde
Institut Langevin, ESPCI Paris
Université PSL, CNRS, 1 rue Jussieu,
F-75005, Paris, France
e-mail: yannick.dewilde@espci.fr

O. Bourgeois *
Institut NEEL, Univ. Grenoble Alpes
CNRS-25 avenue des Martyrs
F-38042 Grenoble, France
e-mail: olivier.bourgeois@neel.cnrs.fr

ABSTRACT

In this work, we propose an experimental set-up to measure the thermal conductivity and specific heat of a single suspended glass fiber, as well as the thermal contact resistance between two glass fibers. By using optical lithography, wet and dry etching and thin film deposition, we prepared suspended glass fibers that are coated by niobium nitride thin film (NbN) used as room temperature thermal transducer. By using the 3ω technique, the thermal conductivity of glass fiber was measured to be 1.1 $W.m^{-1}.K^{-1}$ and specific heat 0.79 $J.g^{-1}.K^{-1}$ around 300 K under vacuum conditions. By introducing exchange gas into the measurement chamber, influence of the gas on the heat transfer was studied, and the convection coefficient h for all the measurement ranges from a pressure of 0.01 hPa to 1000 hPa, over more than five orders of magnitude, has been obtained. By adding a bridging glass fiber on top of two other suspended glass fibers, it was possible to estimate the thermal contact resistance between two glass fibers R_c in the range of 10^7 $K.W^{-1}$ to 10^8 $K.W^{-1}$.

1 Introduction

Nowadays, the energy loss is a common problem world wild. As an example, a large part of the energy consumption goes to heat buildings ($\approx 40\%$ in Europe); the heat leaks being due to bad thermal isolation [1, 2]. One of the solutions for this problem is to reduce the heat loss (by the roof, the walls and the windows) by developing advanced materials, particularly thermal insulation materials for buildings. Most traditional insulation materials have a thermal conductivity between 30 to 50 $mW.m^{-1}.K^{-1}$ at 10°C [3, 4]. Thanks to recent progress in this field, there have been advanced insulation materials developed having thermal conductivity lower than that of traditional insulation material such as aerogel silica showing a thermal conductivity of 18 $mW.m^{-1}.K^{-1}$, or Vacuum Insulation Panels (VIP) based on nanostructured silica or glass fiber with a thermal conductivity as low as 7 $mW.m^{-1}.K^{-1}$. However, current thermal models of these innovative materials predict much lower thermal conductivity in relative disagreement with the one that is measured at the macroscale.

*Corresponding author.

In order to improve the insulating capacity of the composite materials, one must understand all the mechanisms of the heat transfer through the insulation material including convection, conduction in the solid phases and through the air as well as by radiation. In general, the thermal conductivity characterization of insulation materials is based on a macroscopic sample with a size bigger than 10 cm. This characterization technique is enough to give the effective thermal conductivity of the bulk material. However, to further improve the performance of the insulation materials, one needs to have information on the contribution of each individual heat transfer mechanisms at microscopic scale (conduction, convection, radiation) along with each building blocks. In VIP insulating material, the building block is based on glued single glass fibers.

To characterize the heat conduction in one dimensional systems such as micro/nano fibers, different techniques are available, including 3ω technique [5–18], optical heating-electrical thermal sensing technique [19], pulsed laser-assisted thermal relaxation technique [20, 21] and transient electrothermal (TET) technique [22]. Among those techniques, the longitudinal 3ω method is the most widely used for the measurement of suspended individual 1D samples [6, 9]. To implement the 3ω technique, a transducer deposited on top of the suspended structure will serve as a heater and as a thermometer at the same time. This transducer is connected to a current source which supplies an AC current oscillating at an angular frequency 1ω. This heating current will generate a voltage oscillating with an angular frequency 3ω, which is directly connected to the thermal conductivity and specific heat of the specimen. So by measuring this 3ω voltage, we will be able to extract the thermal conductivity and specific heat of the sample.

Besides applications in the study of heat conduction in solid materials, the 3ω technique has been recently applied to study the heat transfer in liquid and gas media as well as developed as a sensor for gas and liquid detection [18, 23, 24]. Most of the previous works are dedicated to the measurement of thermal conductivity of the liquid or sensing the amount of a specific liquid or gas. Recently in 2018, Gao and coworkers have reported on the thermal transport around a micro-wire based on a steady-state hot-wire method [25]. They used a platinum (Pt) wire with a diameter of 25 μm acting as thermometer and heater. By using a DC pulse applied to the Pt wire and measuring the temperature of the Pt wire as function of gas pressure, they were able to calculate the heat convection coefficient at different gas pressure.

Unlike the heat conduction in one dimensional system, the thermal transport at the interface between one dimensional systems is not widely studied yet. In recent years, there have been some experimental works on this problem, for examples, thermal contact resistance between single carbon nanotubes [26], the heat transfer in array of aligned TiO_2 nanotubes [27] and the thermal contact resistance between Pt wires [28]. Besides that, the T-type probe technique [29, 30] appears to be interesting due to its practicalities. In this technique, a hot wire, which is heated by a current, is in contact with one end of a to-be-measured wire, the other end of the to-be-measured wire is in contact to the heat sink. The properties of the sample can be determined by measuring the temperature change on the hot wire before and after being in contact with the sample. To the best of our knowledge, there are no work on the study of the heat convection and conduction at the micro-scale on glass fibers.

In the present work, we propose an experimental set-up to measure thermal conductivity, specific heat of a single suspended micro glass fiber based on 3ω technique. And by placing a micro glass fiber on top of two other suspended ones, we can also measure the thermal contact resistance between two glass fibers based on modified transient electrothermal technique [22] or an "H-type probe" [1]. By introducing to the measurement chamber an exchange gas, we analyzed the influence of the gas pressure on the heat conduction through the convection mechanism. With the proposed experiment, we are able to access the thermal information of the most important building block of the insulation materials in terms of conduction of the solid phase as well as the influence of the gas due to the convection heat transport.

2 Methods

In order to measure the thermal conductivity of a single glass fiber by the 3ω method, first the glass fiber is suspended between two electrodes, then a niobium nitride (NbN) thermometric thin film is deposited on the glass fiber to serve as transducer in the experiment [31]. To fix the fiber on the electrodes, silver paste is used since it is a good thermal and electrical conductor. To keep the fiber suspended, the substrate underneath in silicon is etched to make the electrodes look like pillars. Since a thermometric layer is deposited on the fiber, the pillar-like electrodes have to have a bottleneck shape to ensure that the transducer is electrically isolated from the ground.

2.1 Fabrication process

The fabrication of the sample begins from a Si substrate coated by silicon nitride (SiN) with a size of 1 cm^2. By using sputtering, a layer of WTi/Au (5 nm/100 nm) is deposited on the Si substrate (Fig. 1 a). The WTi/Au

[1] A glass fiber is put on top of other two glass fibers forming an H shape.

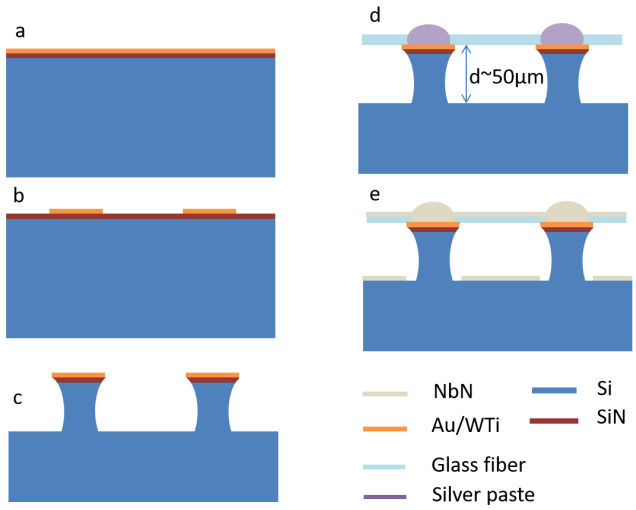

Fig. 1. Micro-fabrication steps for the preparation of suspended glass fibers: a) WTi/Au layer is deposited on the Si substrate, b) Au contacts are structured after the lithography and wet etching, c) contacts in the shape of pillar are obtained after dry XeF_2 etching, d) the glass fiber is suspended and installed on the contacts by silver paste, e) the sample is completed after deposition by sputtering of the NbN thermometer on top of the glass fiber.

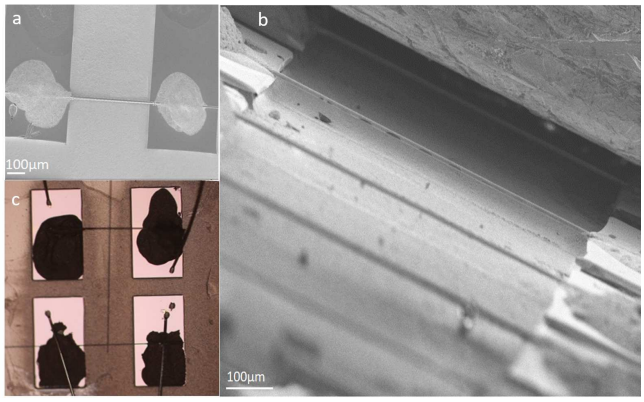

Fig. 2. a) SEM picture of a suspended glass fiber b) SEM picture of the glass fiber obtained under a tilted angle of 90^o showing clearly the suspension between the two electrodes c) optical image of the H-type probe geometry for the measurement of thermal contact resistances.

contacts are obtained by lithography and wet etching of WTi/Au by KI and H_2O_2 solutions as shown in Fig. 1 b. After removing the photoresist by acetone and ethanol, the sample is etched using SF_6 to remove the SiN layer, then loaded immediately into a chamber for vapor etching Si using XeF_2 gas. The step of etching Si by XeF_2 is to obtain contacts with bottleneck shape as shown in Fig. 1 c.

The glass fiber [2] is then placed on top of the contacts and fixed by drops of silver paste as shown in Fig. 1 d. Finally, a 140 nm thick film of NbN thermometer/heater is deposited on the fiber by pulsed DC sputtering. Since the contacts have a shape of bottleneck, the thermometer deposited on the fiber is electrically isolated from the ground as shown in Fig. 1 e. Figure 2 a shows the suspended glass fiber, visualized by Scanning Electron Microscopy (SEM). By tilting the sample at an angle of 90^o, the fiber is observed under SEM as shown in Fig. 2 b. From this picture, we clearly see that the fiber is well suspended and separated from the Si substrate.

Niobium nitride is selected for heater/thermometer in this experiment because it is a well known Mott-Anderson insulator with an increasing resistance as the temperature is decreased [31]. NbN has better sensitivity than other metallic thermometer even at room temperature; indeed the temperature coefficient of resistance (TCR) of NbN at 300 K is about $6\times10^{-3} - 7\times10^{-3}$ K^{-1} in comparison to 2×10^{-3} K^{-1} of Pt thin film thermometer. Moreover, NbN has a much lower electrical conductivity than that of regular metallic thermometers. As a consequence, by using the Wiedemann-Franz law, we can deduce that its thermal conductivity is really low and so this thermometry is perfectly suitable for thermal measurements of low thermal conductivity materials like glass fiber in the geometry of longitudinal 3ω method.

[2]The glass fibers are standard isolation glass supplied by Saint-Gobain Research (SGR).

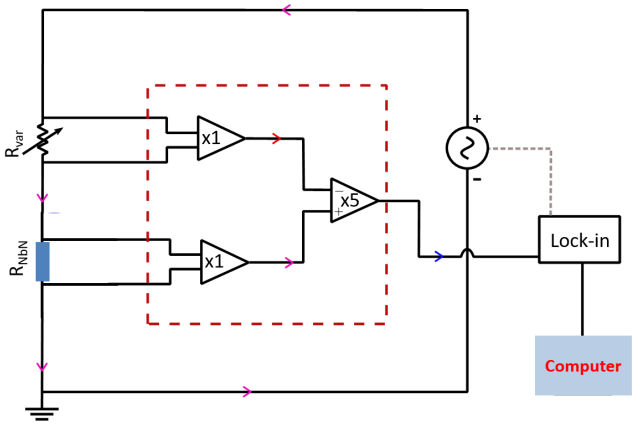

Fig. 3. The electronic set-up dedicated to the 3ω technique is based on a differential bridge. The voltage signal on the thermometer is compared to the voltage on the variable resistor R_{var} in order to extract their difference. By this operation, the dominating 1ω voltage is minimized, and hence the 3ω signal can be extracted with the smallest noise when the variable resistor is set to have the same resistance as the thermometer.

2.2 Experimental protocol of the 3ω measurement techniques

The suspended fiber is heated by an AC current with frequency 1ω, $I = I_0 sin(\omega t)$. Due to Joule heating power $P = P_{dc} + P_{ac} cos(2\omega t)$, the temperature of the transducer increases and oscillates at the angular frequency 2ω, $T = T_{dc} + T_{ac} cos(2\omega t + \varphi)$, leading to the oscillation of the resistance of the thermometer at angular frequency 2ω, $R_{th} = R_0(1 + \alpha_{TCR} T_{dc} + \alpha_{TCR} T_{ac} cos(2\omega t + \varphi))$, where α_{TCR} is the TCR of the transducer. Therefore the voltage generated by the oscillation of the temperature will oscillate at angular frequency 3ω, $V = I_0 R_0 [A sin(\omega t) + \alpha_{TCR} T_{ac} sin(3\omega t + \phi)]$. Since the amplitude of the temperature oscillation T_{ac} is sensitive to both the thermal conductivity and the specific heat of the fiber, by measuring the 3ω voltage, one is able to extract the thermal conductivity and the specific heat of the suspended fiber.

In the experiment, in order to determine the thermal conductivity k and the specific heat c_p of the sample, we made the measurements of $V_{3\omega}$ versus frequency under high vacuum for different samples with different lengths. In a second step, a similar measurement will be performed with the chamber filled with N_2 gas. Under controlled pressure of the gas, a set of $V_{3\omega}$ measurements are made for different pressures. By fitting $V_{3\omega}$ with a mathematical model that will be developed in the following, knowing the value of k and c_p from the measurements under vacuum, the convective heat transfer coefficient between the fiber and the rest of the experimental chamber will be extracted as a function of gas pressure.

2.3 Electronic set-up and thermometer calibration

The fabricated device dedicated to the 3ω technique (as shown in Fig. 2) is mounted on the sample holder loaded into the measurement chamber and pumped to a high vacuum ($p \sim 5\times 10^{-4}$ hPa). In order to have the best sensitivity on the 3ω signal, the thermometer of the fiber is measured using a differential bridge circuit as shown in Fig. 3. In this circuit the NbN thermometer (on the fiber) is connected in series to a variable resistor and connected to a low noise current source. The voltage signals on the NbN thermometer and the variable resistor are extracted from the circuit by comparators in the pre-amplifier. Then this voltage difference is monitored by a lock-in amplifier. Before measuring the 3ω signal, effect from 1ω voltage is canceled by setting the value of the variable resistor to have the minimum 1ω voltage at the output of the pre-amplifier.

For each sample, the resistance of NbN thermometer is first calibrated under high vacuum to obtain the NbN resistance as a function of temperature. Fig. 4 shows the calibration data of the NbN thermometer on the suspended glass fiber. The red square shows the resistance of the thermometer measured with a four point configuration, and the black square shows the data measured with a two point configuration which is easier to implement. The first important point from this data is that the deposited NbN has the expected behaviour since the resistance increases as the temperature decreases. The temperature coefficient of resistance is estimated to be about 6×10^{-3} K^{-1} at room temperature. The second point is that the difference between the two measurement configurations is very small, less than 2% of the absolute value of the resistance. This means that the electrical contact resistance is small; moreover that resistance is thermally coupled to the heat bath, so we do not expect any spurious 3ω signal coming from the contact itself. Hence two point or four point configuration will not make a significant difference. Regarding thermal transport in the thermometer itself, by using the Wiedemann-Franz law, we can estimate the thermal conductance of the NbN layer to be of the order of 10^{-10} $W.K^{-1}$, two orders of

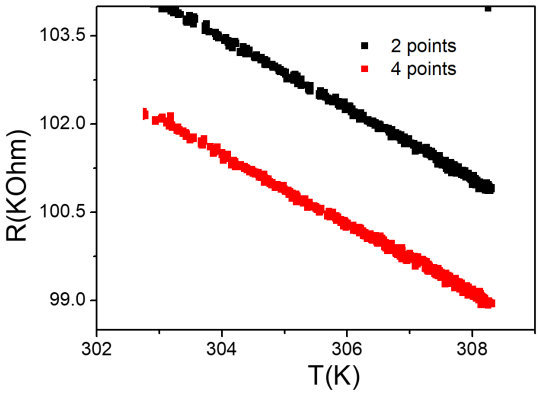

Fig. 4. Calibration of the NbN thermometer deposited on suspended glass fiber. To avoid overheating, an AC current of 100 nA is applied to the thermometer, the calibration is done by measuring the voltage using a lock-in amplifier at different temperatures.

magnitude less that any thermal conductance of glass fibers measured in this work.

3 Mathematical model describing the temperature variation of the suspended fiber

3.1 Solving the 3D heat diffusion differential equation

In the case of suspended glass fiber, the filament can be approximated by a glass rectangular parallelepiped coated by a layer of NbN shown in Fig. 5. This glass parallelepiped is placed at a distance d from the thermal bath at the bottom. The temperature of the thermal bath is set constant at T_0. In order to have the same density of power distributed in the fiber of diameter D_1, as the heater is evaporated on a surface $L\pi D_1/2$, we take $2a = \pi D_1/2$ and $b = D_1/2$, then the surface of the normal section of the fiber is the same as in the real cylindrical glass fiber; here we have investigated glass fibers with a typical diameter $D_1 = 9\mu$m, which yields $a = 7\mu$m and $b = 4.5\mu$m.

The temperature along the fiber $T(x,y,z,t)$ is given by the solution to the 3D heat diffusion differential equation [32]:

$$\frac{\partial^2 T}{\partial x^2}(x,y,z,t) + \frac{\partial^2 T}{\partial y^2}(x,y,z,t) + \frac{\partial^2 T}{\partial z^2}(x,y,z,t) = \frac{1}{D_{diff}}\frac{\partial T}{\partial t}(x,y,z,t) \tag{1}$$

with $D_{diff} = \frac{k}{\rho c_p}$ is the diffusivity of the fiber, k is the thermal conductivity, c_p is specific heat and ρ is the mass density of the fiber. In our experimental condition, the radiation heat loss is neglected.

In order to calculate the solution of Eqn. 1, we need initial and boundary conditions. Due to the symmetry of the problem we only calculate T for $x \geq 0$. The initial condition is : $t = 0$, $T(x,y,z,0) = T_0$ and the boundary conditions are:

$$\begin{cases} y = 0, & T(x,0,z,t) = T_0; \quad y = L, \quad T(x,L,z,t) = T_0 \\ x = 0, & \frac{\partial T}{\partial x}(0,y,z,t) = 0; \quad x = a, \quad -k\frac{\partial T}{\partial x}(a,y,z,t) = h_{2r}(T(a,y,z,t) - T_0) \\ z = 0, & \int_0^a \int_0^L -k\frac{\partial T}{\partial z}(x,y,0,t)\,\mathrm{d}x\,\mathrm{d}y = \frac{P_0}{4}(1-\cos 2\omega t) - \int_0^a \int_0^L h_{2r}[T(x,y,0,t) - T_0]\,\mathrm{d}x\,\mathrm{d}y \\ z = b, & -k\frac{\partial T}{\partial z}(x,y,b) = h_{1r}(T(x,y,b,t) - T_0) \end{cases} \tag{2}$$

with the convection heat transport coefficients h_{1r} for the bottom surface of the fiber and h_{2r} for the other surfaces of the fiber in the rectangular approximation as shown in Fig. 5 where the subscript r stands for rectangular; in vacuum condition $h_{2r} = h_{1r} = 0$. The total electrical power through the heater is $P(t) = R_0 I_0^2 \sin^2 \omega t$ or $P(t) = \frac{P_0}{2}(1-\cos 2\omega t)$ with $P_0 = R_0 I_0^2$; R_0 the resistance of the heater at $T = T_0$ measured in four probe configuration. Here, we used $\frac{P(t)}{2}$ for the heating power, due to the symmetry of the problem. With the small thickness of the NbN layer, we neglected the mass of the heater in the solution of Eqn. 1.

Our model can account for the fact that the sample is placed closed to the bottom of the vacuum chamber ($10\mu m \leq d \leq 100\mu m$) and the convective coefficients are different for the bottom face at $z = b$ and the other faces ($h_{1r} \neq h_{2r}$). The solution for T is then given by:

$$T(x,y,z,t) = T_0 + T_{stat}(x,y,z) + U(x,y,z,t) + U_h(x,y,z,t) \tag{3}$$

with $T_{stat}(x,y,z)$ is the stationary part, $U(x,y,z,t)$ is the transient part and $U_h(x,y,z,t)$ is the periodic part. At the angular frequency 2ω only the determination of $U_h(x,y,z,t) = U_h(x,y,z)e^{2i\omega t}$ is of importance. By using the Fourier method of separation of variables [32], one obtains for $U_h(x,y,z)$:

$$U_h(x,y,z) = -\sum_{n=1}^{\infty}\sum_{m=0}^{\infty} \sin(\lambda_m a)\frac{P_0[(-1)^n - 1]}{aLn\pi}\frac{\sin(\gamma_m y)\cos(\lambda_m x)[\cosh(\alpha_{nm}z) - B_{nm}\sinh(\alpha_{nm}z)]}{\lambda_m a[1 + \frac{\sin(2\lambda_m a)}{2\lambda_m a}][h_{2r} + k\alpha_{nm}B_{nm}]} \tag{4}$$

with $\alpha_{nm} = (\gamma_n^2 + \lambda_m^2 + \frac{2i\omega}{D_{diff}})^{1/2}$, where $\gamma_n = \frac{n\pi}{L}$ and λ_m are solution of $\tan(\lambda_m a) = h_{2r}a/(\lambda_m ak)$ and

$$B_{nm} = (1 + \frac{\alpha_{nm}k}{h_1 r}tanh(\alpha_{nm}b))/(\frac{\alpha_{nm}k}{h_{1r}} + tanh(\alpha_{nm}b))$$

.

The mean averaged temperature on x and y at $z = 0$ is:

$$\bar{U}_h(z=0) = \sum_{n=1}^{\infty}\sum_{m=0}^{\infty}\frac{P_0[(-1)^n - 1]^2}{aLn^2\pi^2}\frac{\sin^2(\lambda_m a)}{(\lambda_m a)^2} \times \frac{1}{[1 + \frac{\sin(2\lambda_m a)}{2\lambda_m a}][h_{2r} + k\alpha_{nm}B_{nm}]} \tag{5}$$

In the real space, the mean temperature is obtained from the following three equations:

$$U_r(z=0) = Re[\bar{U}_h(x,y,0) \times e^{2i\omega t}] = [T_{real}\cos(2\omega t) - T_{im}\sin(2\omega t)]\frac{P_0}{aL\pi^2} \tag{6}$$

$$T_{real} = Re\sum_{n=1}^{\infty}\sum_{m=0}^{\infty}\frac{[(-1)^n - 1]^2}{n^2}\frac{\sin^2(\lambda_m a)}{(\lambda_m a)^2[1 + \frac{\sin(2\lambda_m a)}{2\lambda_m a}][h_{2r} + k\alpha_{nm}B_{nm}]} \tag{7}$$

$$T_{im} = Im\sum_{n=1}^{\infty}\sum_{m=0}^{\infty}\frac{[(-1)^n - 1]^2}{n^2}\frac{\sin^2(\lambda_m a)}{(\lambda_m a)^2[1 + \frac{\sin(2\lambda_m a)}{2\lambda_m a}][h_{2r} + k\alpha_{nm}B_{nm}]} \tag{8}$$

Coming back to the 3ω method, the overall voltage is measured at the two extremities of the filament:

$$V(t) = (R_0 + \delta R)I_0\sin(\omega t) \tag{9}$$

where $\delta R = \left(\frac{dR}{dT}\right)_{T=T_0} \times U_r$. At the 3ω angular frequency, the voltage $V_{3\omega}$ will be related to the temperature oscillation by the relation:

$$V_{3\omega} = \frac{1}{2}\frac{R_0 I_0^3}{aL\pi^2}\left(T_{im}\cos(3\omega t) + T_{real}\sin(3\omega t)\right)\left(\frac{dR}{dT}\right)_{T=T_0} \tag{10}$$

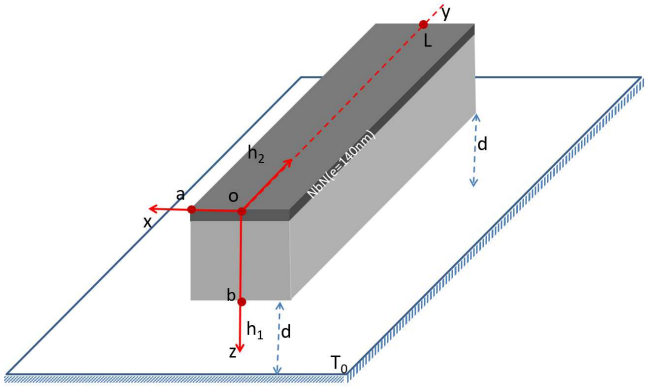

Fig. 5. Model of the glass fiber coated by NbN (of thickness $e = 140$ nm) as a rectangular parallelepiped placed at a distance d from the thermal bath at the bottom, with the convective heat transport coefficients h_{1r} for the bottom surface and h_{2r} for the top and side surfaces, L being the length of the fiber, b the thickness and a the half width of the rectangular parallelepiped.

$$V_{3\omega} = \frac{1}{2}\frac{R_0 I_0^3}{aL\pi^2}\left(\frac{dR}{dT}\right)_{T=T_0}(T_{real}^2 + T_{im}^2)^{1/2}\sin(3\omega t + \phi) \tag{11}$$

with $\tan\phi = \frac{T_{im}}{T_{real}}$.

Experimentally, a root mean square (rms) current is applied and hence the measured modulus of the $V_{3\omega}$ will be given by:

$$(V_{3\omega})_{rms} = \frac{R_0 I_{rms}^3}{aL\pi^2}\left(\frac{dR}{dT}\right)_{T=T_0}(T_{real}^2 + T_{im}^2)^{1/2} \tag{12}$$

This is the crucial equation that will be used later on to fit experimental data and extract the thermal properties of the suspended fiber. Under high vacuum conditions, $h_{2r} = h_{1r} = 0$, we obtained the same equations for the phase and the RMS modulus as in Lu's work [6]. Finally, the value of k and c_p will be obtained by fitting the experimental data of $(V_{3\omega})_{rms}$ as a function of the angular frequency using Eqn. 12.

If exchange gas is introduced in the measurement chamber, then we will need the value of h_{1r} and h_{2r}, keeping the same k and c_p as obtained from vacuum conditions, to fit the $(V_{3\omega})_{rms}$ as a function of the angular frequency ω. For this, we need to have a very clear estimation of h_{1r} and h_{2r}, if one wants to use Eqn. 12 under gas pressure.

3.2 Evaluation of the convection heat transport coefficients

In the previous section, to solve the differential equation of the heat diffusion, the glass fiber was approximated as a rectangular parallelepiped, an approximation that eases to find the solution of the $V_{3\omega}$, with h_{1r} and h_{2r} the coefficients of convection corresponding to different surfaces that need to be calculated precisely.

In the heat transfer theory of rarefied gas at rest, the calculations are made in th symmetric cylindrical geometry for instance to evaluate the convection between a cylindrical fiber of diameter D_1 at a temperature T_1 and an external concentric cylinder of diameter D_2 at a temperature T_2 (with $D_2 > D_1$). However, in our experimental case, the geometry of the glass fiber inside the measurement chamber as depicted in Fig. 6 is neither symmetric nor cylindrical. If the glass fiber used in this work is cylindrical, it is however suspended at a distance d from the flat Si substrate that is connected to the thermal bath with 10 μm$\leq d \leq 100\mu$m. Therefore, we have neither a total cylindrical symmetry nor a planar symmetry. However, the dimensions of the experimental chamber ($D_2 \simeq 2$ cm) is much larger than the sample width justifying that the calculation of h, made in the cylindrical symmetry, is the most appropriate one [33]. Then in order to calculate h_{1r} and h_{2r} we need in fact to solve three problems, 1-find the right geometry for the system (fiber and chamber) allowing the use of the calculations of h_{1c} and h_{2c} in the symmetric cylindrical geometry (the subscript c standing for cylindrical), 2-calculating h_{1c} and h_{2c} for various pressures, 3-find the correspondence between the two geometry (rectangular and cylindrical), meaning a relation between $h_{1c,2c}$ and $h_{1r,2r}$.

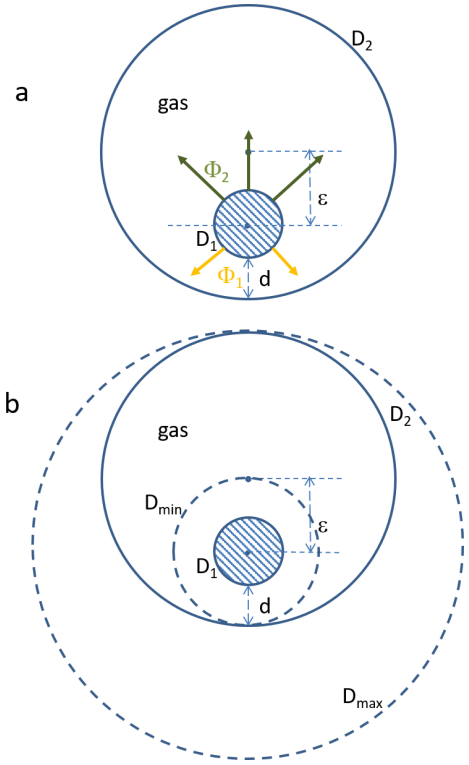

Fig. 6. Approximate model for the convection heat transport. a) D_1 is the diameter of the fiber (inner cylinder), D_2 is the diameter of the experimental chamber (outer cylinder), ε is the separation between the center of the fiber and the center of the experiment chamber, d is the distance from the bottom of the fiber to the bottom of the experimental chamber, Φ_1 in orange and Φ_2 in green are the heat flux respectively to the bottom or to the top of the chamber. b) schematic showing the assumption of the double cylindrical geometry where the heat flux to the top of the chamber Φ_2 is calculated using the cylinder D_{max} and the heat flux to the bottom of the chamber Φ_1 is calculated using the cylinder D_{min}.

3.2.1 h_{1c} and h_{2c} in a cylindrical geometry

In a purely conductive regime, where k_{gas} is the thermal conductivity of a gas filling the outer cylinder, the rate of total heat flow between the two cylinders of length L and diameter D_1 and D_2, as depicted in Fig. 6 a, can be exactly calculated without any assumption on the geometry using the following equation [34]:

$$\Phi = \pi D_1 L \frac{k_{gas}}{D_1} \frac{2(T_2 - T_1)}{cosh^{-1}[(D_1^2 + D_2^2 - 4\varepsilon^2)/2D_1D_2]} = h_c S_1 \Delta T \tag{13}$$

where ε is the vertical eccentricity of the inner cylinder and $S_1 = \pi D_1 L/2$, the surface of the fiber.

A reasonable approximation can be made where the flux Φ is expressed as a sum of two heat fluxes. In this approximation, the heat flowing from the fiber to the surrounding chamber is divided in two parts. One part will be the upper heat flux, Φ_2, that is exchanged between half of the surface S_1 with the top part of the chamber (approximated as a cylindrical chamber of diameter $D_{max} = D_2 + 2\varepsilon$), and the second part, the lower heat flux Φ_1, that is exchanged between half of the surface S_1 with the bottom part of the chamber (approximated as a cylindrical chamber of diameter $D_{min} = D_1 + 2d$). The schematic describing this approximation is shown in Fig. 6 b. In each situation, the heat flux $\Phi_{1,2}$ will be associated with an exchange coefficient $h_{1c,2c}$ following :

$$\Phi_{1,2} = h_{1,2} \frac{S_1}{2} \Delta T \tag{14}$$

knowing that the total heat flux is expressed through: $\Phi = \Phi_1 + \Phi_2$. We can deduced from Eqn. 14 a mean value for h:

$$h_c \simeq \frac{h_{1c} + h_{2c}}{2} \tag{15}$$

We can now compare the final value for h that can be calculated using Eqn. 15 to the one calculated using the approximation made to obtain Eqn. 15; h_{1c} and h_{2c} being calculated using Eqn. 13 replacing D_2 by D_{min} for h_{1c} and by D_{max} for h_{2c} along with $\varepsilon = 0$ to be in accordance with our approximations.

Considering the typical sample prepared for this experiment, $D_1 = 9$ μm, $d = 71$ μm, $D_2 = 2$ cm, $\varepsilon = 1$ cm, $k_{gas} = 2.4$ W.cm^{-1}.K^{-1}. The coefficient h_c obtained from Eqn. 15 are then $(h_{1c} + h_{2c})/2 = 1292$ W.m^{-2}.K^{-1} a very close value to the h_c coefficient calculated from Eqn. 13: $h_c = 1367$ W.m^{-2}.K^{-1}. Within a reasonable accuracy this calculation shows that our assumption of a double cylindrical geometry for the calculation of h coefficients is good enough, and justifies its extension to the convection regime.

3.2.2 The h coefficients in the convective regime

To estimate the convection coefficient, one needs also to discuss the different regimes of heat transfer through the gas since it will affect the limit used for the calculation. In these experiments, since pressure below the atmosphere is used, the heat transfer from the fiber to the gas will be done in the limit of rarefied gas; indeed, the case of atmospheric pressure is not the most interesting one for this study. By rarefied gas, we mean that the molecular mean free path λ [3] is not small as compared to the characteristic dimension D; here D can be, for instance, the diameter of the filament $D_1 = 9$ μm. Since the studies of Maxwell on this problem [35], numerous analytical solutions have been given, all of them depending on the Knudsen number $Kn = \frac{\lambda}{D_1}$ [36]. Four different regimes of heat transfer can be distinguished: the free molecule regime ($Kn \geq 10$), the transition regime ($10 \geq Kn \geq 0.1$), the slip flow regime ($0.1 \geq Kn \geq 0.01$) and the continuum or hydrodynamic regime ($Kn \leq 0.01$) [33].

3.2.3 h_{1r} and h_{2r} calculations in the rectangular geometry

In this part, we will calculate h_{1r} and h_{2r} convection coefficients calculated in rectangular conditions as used in the final equations describing the temperature oscillation Eqn. 6, Eqn. 7 and Eqn. 8 as a function of h_{1c} and h_{2c} convection coefficients calculated in cylindrical conditions. In the calculation of the $(V_{3\omega})_{rms}$ we used a model where the area of the normal section of the sample was $2ab$ (see Fig. 5), but the real sample is a cylinder with diameter D_1, both of them have the same length L. If we take $2a = \pi D_1/2$ and $b = D_1/2$, we have the same density of power per m^3 in cylindrical or rectangular condition, which is necessary in vacuum conditions. But when the surface of the sample exchanges power with gas, our approximation is working, as we explained, if $ab = \pi D_1^2/8$ along with $\frac{\pi D_1 L h_{2c}}{2} = 2aLh_{2c} = (2a+2b)Lh_{2r}$, then a simple geometrical correspondence gives the relation between h_{1r}, h_{2r} and h_{1c}, h_{2c}:

$$h_{1r} = h_{1c} \tag{16}$$

$$h_{2r} = \frac{h_{2c}}{1 + \frac{2}{\pi}} \tag{17}$$

Now, in the following, h_{1c} and h_{2c} will be calculated for different ranges of pressure. For a diatomic gas in the free molecule regime and in the transition regime (low pressure) the convection coefficient is given by [33]:

$$h_{1,2}^{LP} = \frac{h_{FM}}{1 + \frac{4\times45\times0.5\alpha_r D_1}{15\times38\lambda} ln(\frac{D_{min,max}}{D_1})} \tag{18}$$

$D_{min,max}$ being defined as in Fig. 6. In Eqn. 18, h_{FM} is the convection coefficient in the free molecule regime given by:

$$h_{FM} = \frac{\alpha_r(\gamma+1)}{2(\gamma-1)} \sqrt{\frac{R_0}{2\pi M T_2}} p \tag{19}$$

---

[3] The mean free path at a pressure P (as compared to the atmospheric pressure P_a) is given by the following equation $\lambda = 5.88 \times 10^{-3} P_a/P \sqrt{\frac{T}{T_0}}$ where T_0 is the room temperature.

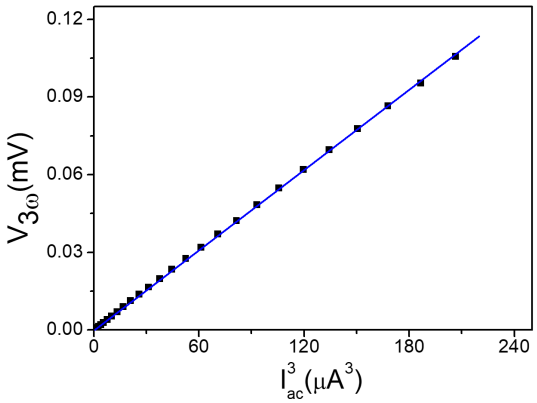

Fig. 7. $V_{3\omega}$ versus RMS heating current at the frequency of 1.3 Hz. The linearity of the voltage signal measured by the lock-in amplifier with the cube of the RMS current is showing that no over-heating is present during the measurement.

where $\alpha_r = \frac{\alpha}{1+(1-\alpha)\frac{D_1}{D_2}}$ with α is the accommodation coefficient closed to 0.93 (see Appendix A), γ is the ratio of the specific heats at constant pressure and constant volume (for N_2 $\gamma = 1.4$), M is the molecular mass of N_2 in kg per mole, T_2 is the temperature of the measurement ($T_2 = 298$ K), p is the pressure of the gas in Pascal and R is the molar gas constant ($R = 8.314$ J.mol^{-1}.K^{-1}).

In the slip flow regime, with $p \geq 3$ hPa (corresponding to a mean free path $\lambda = 20$ μm), we used a calculation proposed by Hadj-Nacer et al. [37]:

$$h_{1,2}^{HP} = \frac{15\lambda p}{4D_1}\sqrt{\frac{2T_2R_0}{M}}\frac{2(T_1^{1.5}-T_2^{1.5})}{3T_2^{1.5}(T_1-T_2)[ln(\frac{D_{min,max}}{D_1})+A\frac{2\lambda}{D_1}(\frac{T_1}{T_2}+\frac{D_1}{D_{min,max}})]} \tag{20}$$

with $A = (\frac{2-\alpha}{\alpha}+0.17)\frac{\sqrt{\pi}}{P_r}\frac{\gamma}{\gamma+1}$ where P_r is Prandtl number, for N_2 at $T_2 = 298$ K $P_r = 0.71$. For each range of pressure, $h_{LP}^{1,2}$ and $h_{HP}^{1,2}$ have to be calculated for different surfaces of the samples.

As a conclusion for this part, depending of the regime of pressure, h_{1c} and h_{2c} will be equaled to either $h_{1,2}^{LP}$ in the low pressure regime or $h_{1,2}^{HP}$ in the high pressure regime as described in Eqn. 18 and Eqn. 20.

4 Results

4.1 Thermal conductivity and specific heat of glass fiber

The first test we have to do in the measurement of thermal conductivity and specific heat of glass fiber is to measure the dependency of the 3ω signal on the amplitude of the applied RMS current. Fig. 7 represents the 3ω voltage signal as a function of I_{ac}^3. The data shows a linear behavior meaning that in this measurement range the fiber is not over-heated. This linear dependency with the cube of the current is the confirmation of the proper functioning of the method and device. Then to extract the thermal properties (k and c_p), the $V_{3\omega}$ signal is measured as a function of the frequency of the heating current as shown in Fig. 8. Red circles represent the experiment data, black line is the adjustment of the data by using Eqn. 12 with fitting parameters k and c_p. One can noticed that the device has the expected response to the change of frequency as predicted by 3ω technique modelling through Eqn. 12 giving high confidence in the thermal conductivity and specific heat extracted from the experiment.

The measurements have been performed on many different fibers having various sizes. For each one, we fit the experimental data to get the thermal conductivity and specific heat of the glass fiber as the fitting parameters using Eqn. 12. By doing a statistical analysis on all the devices (more than twenty samples were measured), we have obtained an average value of the thermal conductivity of glass fiber about 1.08 ± 0.12 W.m^{-1}.K^{-1} and specific heat about 0.78 ± 0.17J.g^{-1}.K^{-1}, which are in very good agreement with the values found in literature [38–41]. It can be noticed that the thermal conductivity is obtained with little scattering, though the specific heat shows a larger dispersion. This is coming from the fact that in the 3ω technique, thermal conductivity is measured with lesser experimental error than the specific heat since it is estimated by fitting the high frequency part of the $V_{3\omega}$ measurement [42, 43].

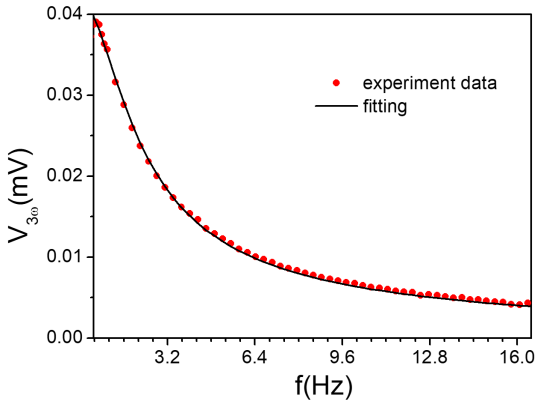

Fig. 8. $V_{3\omega}$ voltage as a function of the heating current frequency for bias current of $I = 3.94\mu$A. The red circles are the experimental data and the black line is the fitting curve using Eqn. 12 that will give the values of thermal conductivity and specific heat; in the case of this sample, we find $k = 1.05$W.m^{-1}.K^{-1} and $c_p 0.80$ J.g^{-1}.K^{-1}.

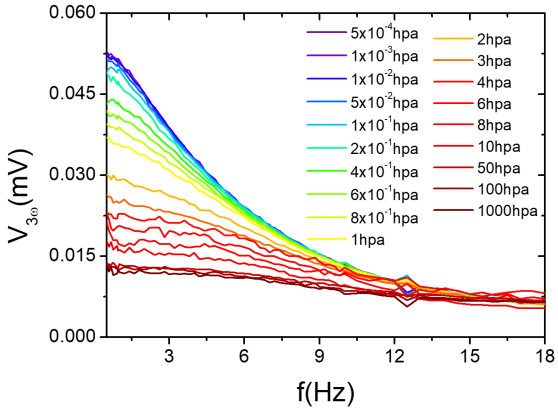

Fig. 9. $V_{3\omega}$ signal versus frequency at different gas pressures. The $V_{3\omega}$ is first collected at high vacuum, then the measurement chamber is filled gradually with N_2. At each controlled pressure, $V_{3\omega}$ is measured as function of frequency.

Figure 9 shows a set of $V_{3\omega}$ voltages as a function of frequency measured for different pressures of N_2 from high vacuum (10^{-4} hPa to ambient pressure 1000 hPa). These data clearly show a dependence of the $V_{3\omega}$ signals to the pressure of the gas; the $V_{3\omega}$ voltages decreasing as the pressure increases due to a decrease of the temperature oscillation. This is expected since by adding gas an extra thermalization path is provided.

To perform the $V_{3\omega}$ data treatment using Eqn. 12, we will set the value of h_{1r} to the one that is calculated from the model described in the prior section using Eqn. 16, Eqn. 18 and Eqn. 20, keeping h_{2r} as the only free parameter. For obtaining the convection coefficient h_{2r} at various pressure, the procedure described below has been used. First, under vacuum condition ($h_{1c} = h_{2c} = 0$), the fitting of $(V_{3\omega})_{rms}$ will give the intrinsic thermal properties of the glass fiber k and c_p, and second for experiments done under gas pressure, the $(V_{3\omega})_{rms}$ is fitted using Eqn. 12 with the convection coefficient h_{2r} as free parameter. The comparison of the experimental value of h_{2r} with the model required to consider two situations. In the low pressure case, when $p \leq 3$ hPa, the experimental value h_{2r} is compared to the calculated value h_2^{LP} as obtained from Eqn. 17 and Eqn. 18. For the high pressure limit, when $p \geq 3$ hPa the experimental value h_{2r} is compared to the calculated value h_2^{HP} given by Eqn. 17 and Eqn. 20.

These results are presented in Fig. 10. There is a very good agreement on all the measurement ranges of pressure between the value of h_2 obtained by fitting the Eqn. 12 to our experimental data, and h_2 calculated with Eqn. 18 or Eqn. 20. As a conclusion, for a wire of about 10 μm, the variation of the convection coefficients with pressure can be well described by classical analysis of convection processes. At atmospheric pressure, a value of 300 W.m^{-2}.K^{-1} is found for the convective coefficient much bigger than for macroscale surface where the h coefficient is equal to 10 W.m^{-2}.K^{-1} [4,44]. This value can be compared to several existing values in the literature of microfabricated structures from 35 W.m^{-2}.K^{-1} measured on membranes by Jain et al. [45] and the one found

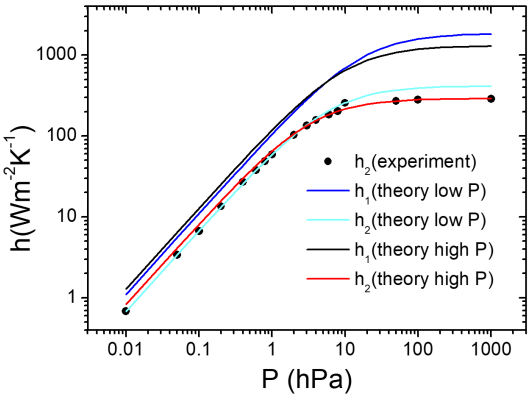

Fig. 10. Convection coefficients obtained by fitting our experimental data in comparison to the calculated values obtained from model detailed in the present work. The black circles represent the convection coefficient h_{2r} obtained from the fit of the experimental data; the calculated coefficients h_1 and h_2 from the model are also presented for comparison: the black line is the convection coefficient h_1 in the high pressure limit, the dark blue line corresponds to h_1 in the low pressure limit; the red line is the convection coefficient h_2 obtained for high pressure, and the light blue line for low pressure.

by Gao et al. where a coefficient of 600 W.m^{-2}.K^{-1} has been measured on suspended platinum wire [25]; values even much higher have been found in the case of carbon nanotubes [46]. The difference could originate from the fact that the different micro or nano-structures do not have the same surface roughness and dimensions, but also because Gao and coworkers, for instance, have used an experiment involving much higher ΔT along with different data treatment techniques. As a conclusion, this experiment is of interest not only to evaluate h factor in the case of MEMs and suspended probes for scanning microscopy, but also to show that a suspended glass fiber may serve as a possible sensitive device for gas sensing for pressure p below 10 hPa.

4.2 Thermal contact resistance between two glass fibers

The last part of this work is dedicated to the estimation of the contact thermal resistance that may exist between two glass fibers. This thermal resistance is playing a significant role in all the applications for thermal isolation involving glass fibers, especially in rock-wool materials. The following is then detailing the experiment and its modelling along with the experimental results.

4.2.1 Thermal contact resistance model

In order to get access to the thermal resistance when two glass fibers are put in contact, few suspended glass fibers are installed in parallel. Then, we select two suspended fibers one next to the other, and on these two fibers, we place another fiber at the middle of the two fibers as shown in Fig. 11. This configuration of the three fibers forms a H-like structure, referred to as H-type probe in the following [47]. In this measurement, one suspended fiber will be used as heating wire (L_1), and the other one acts as sensing wire (L_2). By measuring the temperature of the heating wire and sensing wire at the thermal equilibrium state, we can determine the thermal contact resistance between the top fiber and the two fibers underneath as depicted in Fig. 11; this means that we will actually measure the thermal contact between a glass fiber coated with NbN and a bare glass fiber.

In this development, a DC current is first applied to the heating wire (L_1). Due to Joule heating, the fiber L_1 will be heated to an equilibrium temperature with $T_{1max} = T_1$ at the center of the fiber L_1. Then due to the heat transfer through the crossing fiber, the fiber L_2 is slightly heated to an equilibrium state with the maximum temperature at the center $T_{2max} = T_2$. By measuring the temperature T_1 and T_2,the thermal contact resistance can be extracted.

The thermal model of the contact resistance is detailed below. Based on the thermal resistance circuit presented in Fig. 12, the heat flux $\dot{Q}_c$ from fiber L_1 to fiber L_2 through the crossing fiber L_3 is given by:

$$\dot{Q}_c = \frac{T_1 - T_2}{2R_c + R_3} \tag{21}$$

where R_c and R_3 are the thermal contact resistances between glass fibers and thermal resistance of fiber L_3

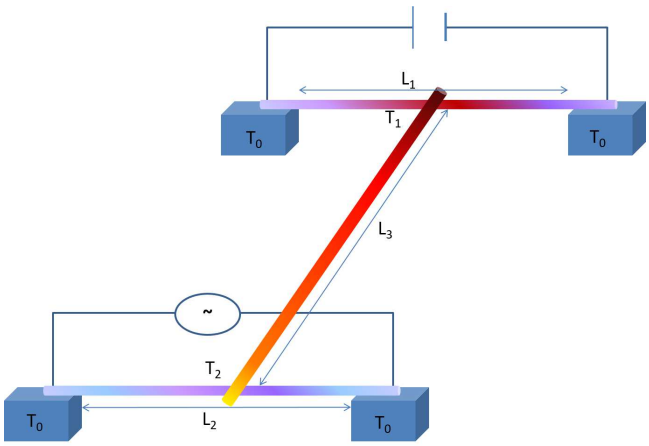

Fig. 11. Scheme of the H-type experiment: L_3 is the crossing fiber (of 1.05 mm length) connecting thermally the two other fibers $L_1 = 0.39$ mm and $L_2 = 0.5$ mm ; L_1 is heated by a DC current, a voltmeter is used to measure the voltage on the heating fiber and get its temperature T_1; the sensing fiber L_2 is excited by an AC current, and a lock-in amplifier is used to measure the voltage on the sensing fiber and gets its temperature T_2. The temperature gradient along the fibers will determine the thermal resistance of the contact between the fibers.

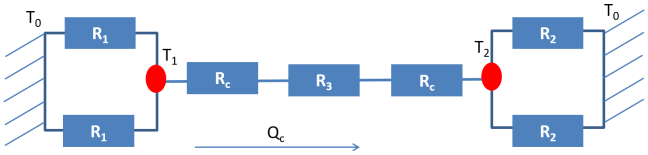

Fig. 12. Thermal resistance circuit representing the H-type experiment. T_0 is the temperature of the thermal bath, T_1 is the temperature at the contact between fiber L_1 and fiber L_3, $T_2$the temperature at the contact between fiber L_2 and fiber L_3, R_c is the thermal contact resistance between two glass fibers which is supposed to be the same for different fiber pairs, R_1 and R_2 are halves of the thermal resistance of the fibers L_1 and L_2, and R_3 is the thermal resistance of the fiber L_3.

respectively. Then the heat flux through the sensing fiber L_2 to thermal bath is given by:

$$\dot{Q}_2 = \frac{2(\mathrm{T}_2 - \mathrm{T}_0)}{\mathrm{R}_2} \tag{22}$$

where R_2 is a half of the thermal resistance of the fiber L_2. Since the heat flux through L_3 is equal to the heat flux through L_2 then:

$$\frac{T_1 - T_2}{2R_c + R_3} = \frac{2(T_2 - T_0)}{R_2} \Rightarrow R_c = \frac{R_2(T_1 - T_2)}{4(T_2 - T_0)} - \frac{R_3}{2} \tag{23}$$

Substituting $R_3 = L_3/(k_3 A_3)$ in to the above equation, the thermal contact resistance is found to be:

$$R_c = \frac{L_2(T_1 - T_2)}{8k_2 A_2(T_2 - T_0)} - \frac{L_3}{2k_3 A_3} \tag{24}$$

where k_3, A_3 and k_2, A_2 are the thermal conductivities and cross-section of the crossing-fiber L_3 and the sensing fiber L_2 respectively. Assuming that the fibers have the same thermal conductivity and diameter ($k_2 = k_3$ and $A_2 = A_3$), the thermal contact resistance is written in a simpler form:

$$R_c = \frac{1}{2k_3 A_3}\left(\frac{L_2(T_1 - T_2)}{4(T_2 - T_0)} - L_3\right) \tag{25}$$

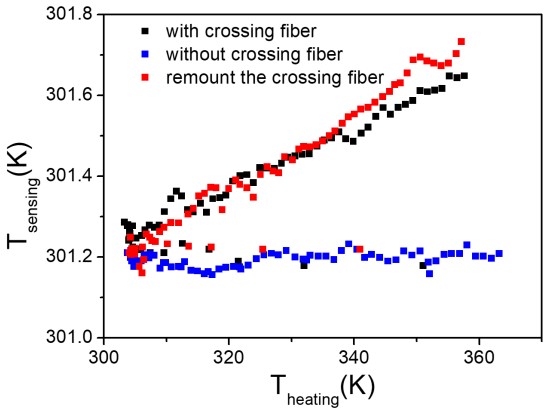

Fig. 13. Temperature on the sensing side versus temperature on the heating side when a fiber is deposited across the two other fibers. The blue squares represent data after removing the crossing-fiber to serve as a reference, as expected, no heating can be detected. The red squares represent data after re-mounting the crossing-fiber to show the reproducibility of the experiment.

Since k_3, A_3, L_2, L_3 and T_0 are known parameters, when T_1 and T_2 are measured, the thermal contact resistance can be calculated by using Eqn. 25.

4.2.2 Thermal contact resistance between glass fibers

In the experimental set up to estimate the thermal contact resistance, we sweep the heating current I_{DC} from 1 μA to 70 μA with step of 1 μA and collect the temperature on both heating and sensing sides. The data is shown in Fig. 13. From this data, we can clearly see heating effect on the sensing fiber with the appearance of the crossing-fiber (black squares in Fig. 13). This heating effect is confirmed to be due to the heat transfer through the crossing-fiber, since the sensing fiber is not heated when the fiber bridging the two others is not present (blue squares in Fig. 13). The reproducibility is confirmed by mounting again the crossing-fiber (red squares in Fig. 13) and obtaining the same results.

From the data presented in Fig. 13, we applied the Eqn. 25, with the known dimension of the fiber as well as the thermal conductivity of glass fiber ($k = 1.1$ W.m^{-1}.K^{-1}) to obtain the thermal contact resistance $R_c \approx 5 \times 10^7$ K.W^{-1}. This value is in good agreement with what has been observed in SThM thermal contact measurements [48, 49]. While the crossing cylindrical fibers between which the contact is made in our experiment have a diameter of 9 μm, their surface exhibits sub-nanometer roughness over micrometer distances due to the drawing process by which they are produced [50]. It is thus likely that they are in contact only through nanometer-sized channels in vacuum. Note that the thermal contact resistance measurement that we perform does not discriminate between the conductive and the near-field radiative channel. However, it is expected that the latter will contribute very little since experimental measurements of the radiative thermal conductance as a function of the distance between two objects exhibits a dramatic increase when solid-solid contact is established [51, 52].

5 Conclusion

We have developed an experimental method for the measurements of thermal conductivity and specific heat of a single suspended glass fiber, thermal contact resistance between two glass fibers and convection through the exchange gas at different gas pressures. The measurements based on the 3ω technique have shown that thermal conductivity and heat capacity of glass fiber are the same as that of regular glass ($k = 1.1$ W.m^{-1}.K^{-1}, $c_p = 0.79$ J.g^{-1}.K^{-1}). The convection heat transfer was analyzed by changing the pressure of the exchange gas in the measurement chamber. With the same sample, it was possible to perform different measurements and get the contribution in thermal transport from different heat transfer mechanisms in single glass fiber. The 3ω experiment allowed to extract the convection coefficient from the fiber to the rest of the experimental chamber at different pressures in good agreement with the various models of heat transfer through a gas. Finally, by using an H-type technique, the thermal contact resistance has been measured with a value in the order of 5×10^7 K.W^{-1}. These observations will contribute to estimate which heat transfer mechanisms is playing the key role in insulation material (conduction, convection or contact resistance).

Acknowledgements

The authors thank the technical support and discussions provided by the Nanofab, Pôle Capteur, Pôle électronique, Pôle cryogenic facilities in Institut Néel. The authors acknowledge support the Laboratoire d'excellence LANEF in Grenoble (No. ANR-10-LABX-51-01), and from Saint Gobain Research Paris for providing the glass fibers. This work also received financial support from LABEX WIFI (Laboratory of Excellence within the French Program Investments for the Future) under references ANR-10-LABX-24 and ANR-10- IDEX-0001-02 PSL*, and Agence Nationale de la Recherche (ANR), Project CarISOVERRE under reference ANR-16-CE09-0012.

Appendix A: Coefficient of thermal accommodation

In order to calculate the heat transfer from the heater, it is necessary to know the flux of energy and momentum carried by the molecules of gas impinging on the surface and then reflected from it. A coefficient of thermal accommodation is then defined as [33, 36]:

$$\alpha = \frac{T_r - T_i}{T_s - T_i} \tag{26}$$

with T_r and T_i are the temperatures of the reflected and incident gas streams, respectively; T_s is the temperature the molecular stream leaving the surface would have, if this stream were to carry the same mean energy as a stream issued from a gas in equilibrium at T_s. As an example, from experimental data obtained for a fiber of W in nitrogen gas: $0.6 \leq \alpha \leq 0.95$ at room temperature [33].

Nomenclature

a Half width of the thermometric NbN strip.
b Thickness of the SiO_2 fiber in the rectangular approximation.
c_p Specific heat.
d Distance from the bottom of the glass fiber to the Si surface.
e Thickness of the NbN strip.
f Frequency of the electrical current.
h Convection coefficients, generic name.
h_1 Convection coefficient of the bottom of the fiber.
h_2 Convection coefficient of the top and sides of the fiber.
h_{1c} Convection coefficient h_1 in cylindrical condition.
h_{2c} Convection coefficient h_2 in cylindrical condition.
h_{1r} Convection coefficient h_1 in rectangular condition.
h_{2r} Convection coefficient h_2 in rectangular condition.
$h_{1,2}^{LP}$ Convection coefficient $h_{1,2}$ in low pressure condition.
$h_{1,2}^{HP}$ Convection coefficient $h_{1,2}$ in high pressure condition.
k Thermal conductivity.
k_2 Thermal conductivity of fiber L_2.
k_3 Thermal conductivity of fiber L_3.
p Pressure in the measurement chamber.
x, y, z and t Space and time coordinates.
A_2 Cross section of fiber L_2.
A_3 Cross section of fiber L_3.
D_{diff} The diffusivity of the fiber materials.
D_1 Diameter of the glass fiber.
D_2 Diameter of the measurement chamber.
I Electrical current.
I_0 Amlitude of the electrical current.
I_{rms} Root mean square of the electrical current.
Kn Knudsen number.
L Length of the glass fiber.
L_1 Length of the glass fiber 1.
L_2 Length of the glass fiber 2.

L_3 Length of the glass fiber 3.
M The molecular mass.
P Electrical power.
P_a Pressure in the measurement chamber.
P_{ac} The oscillating part of the heating power.
P_{dc} The constant part of the heating power.
P_0 Amplitude of the electrical power.
$\dot{Q}_2$ Heat flux through the fiber L_2.
$\dot{Q}_c$ Heat flux through the fiber L_3.
R The molar gas constant.
R_0 Resistance of the transducer at $T = T_0$.
R_1 Half of the thermal resistance of the fiber L_1.
R_2 Half of the thermal resistance of the fiber L_2.
R_3 Thermal resistance of fiber L_3.
R_c Thermal contact resistance.
R_{th} Resistance of the transducer as function of time.
S_1 Surface area of the fiber.
T Temperature.
T_0 Temperature of the thermal bath.
T_1 Temperature at the contact between fiber L_1 and fiber L_3.
T_{1max} Maximum of the temperature distribution on the fiber L_1 due to Joule heating.
T_{2max} Maximum of the temperature distribution on the fiber L_2.
T_2 Temperature at the contact between fiber L_2 and fiber L_3.
T_{ac} The oscillating part of temperature gradient.
T_{dc} The constant part of the temperature gradient.
$T_{heating}$ the temperature on the heating fiber L_1.
T_i Temperatures of the incident gas stream.
T_im The imaginary part of the temperature.
T_r temperatures of the reflected gas stream.
T_{real} The real part of the temperature.
T_s The temperature of the molecular stream leaving the surface.
$T_{sensing}$ The temperature on the sensing fiber L_2.
T_{stat} Stationary part of the temperature.
$V_{3\omega}$ 3ω voltage signal.
$(V_{3\omega})_{rms}$ Root mean square of the 3ω voltage signal.
U Transient part of the temperature gradient.
U_h Periodic part of the temperature oscillation.
$\bar{U}_h$ The complex mean temperature.
U_r The mean temperature in the real space.
α_{TCR} Temperature coefficient of the resistance.
α Coefficient of thermal accomodation.
γ The ratio of the specific heats at constant pressure and constant volume.
λ Molecular mean free path.
ε The separation between the center of the fiber and the center of the experiment chamber/vertical eccentricity
ω Angular frequency of the heating current.
ϕ Phase lag of the 3ω voltage signal.
ρ Mass density of the fiber.
Φ Total heat flow between the fiber and the chamber.
Φ_1 Total heat flow between two concentric cylinders with diameters D_1 and $D_{min} = D_1 + 2\varepsilon$.
Φ_2 Total heat flow between two concentric cylinders of diameters D_1 and $D_{max} = D_1 + 2d$.

References

[1] Allouhi, A., Fouih, Y. E., Kousksou, T., Jamil, A., b, Y. Z., and Mourad, Y., 2015. "Energy consumption and efficiency in buildings: current status and future trends". J. Cleaner Prod., 109, pp. 118–130.

[2] Tanica, M., Stankovica, D., Nikolica, V., Nikolica, M., Kostica, D., Milojkovica, A., Spasica, S., and Vatin, N., 2015. "Reducing energy consumption by optimizing thermal losses and measures of energy recovery in preschools". Procedia Engineering, 117, pp. 919—932.

[3] Jelle, B., 2011. "Traditional, state-of-the-art and future thermal building insulation materials and solutions – properties, requirements and possibilities". Energy Build, 43, pp. 2549–2563.
[4] Langlais, C., and Klarsfeld, S., 2004. "Isolation thermique à température ambiante. propriétés.". Techniques de l'Ingénieur, 9, p. 960.
[5] Cahill, D. G., 1990. "Thermal conductivity measurement from 30 to 750 k: the 3ω method". Rev. Sci. lnstrum., 61, p. 802.
[6] Lu, L., Yi, W., and Zhang, D., 2001. "3ω method for specific heat and thermal conductivity measurements". Rev. Sci. lnstrum., 72, pp. 2996–3003.
[7] Choi, T. Y., Poulikakos, D., Tharian, J., and Sennhauser, U., 2006. "Measurement of the thermal conductivity of individual carbon nanotubes by the four-point 3ω method". Nano Lett., 6, pp. 1589–1593.
[8] Hou, J., Wanga, X., Vellelacheruvu, P., and Guo, J., 2006. "Thermal characterization of single-wall carbon nanotube bundles using the self-heating 3ω technique". J. Appl. Phys., 100, p. 124314.
[9] Bourgeois, O., Fournier, T., and Chaussy, J., 2007. "Measurement of the thermal conductance of silicon nanowires at low temperature". J. Appl. Phys., 101, p. 016104.
[10] Heron, J. S., Fournier, T., Mingo, N., and Bourgeois, O., 2009. "Mesoscopic size effects on the thermal conductance of silicon nanowire". Nano Lett., 9, pp. 1861–1965.
[11] Schiffres, S., and Malen, J., 2011. "Improved 3ω measurement of thermal conductivity in liquid, gases,and powders using a metal-coated optical fiber". Rev. Sci. lnstrum., 82, p. 064903.
[12] Sikora, A., Ftouni, H., Richard, J., Hébert, C., Eon, D., Omnes, F., and Bourgeois, O., 2012. "Highly sensitive thermal conductivity measurements of suspended membranes (sin and diamond) using a 3ω-völklein method". Rev. Sci. Instrum., 83(5), p. 054902.
[13] Sikora, A., Ftouni, H., Richard, J., Hébert, C., Eon, D., Omnes, F., and Bourgeois, O., 2013. "Erratum: "highly sensitive thermal conductivity measurements of suspended membranes (sin and diamond) using a 3ω völklein method" [rev. sci. instrum. 83, 054902 (2012)]". Rev. Sci. Instrum., 84, p. 029901.
[14] Finefrock, S. W., Wang, Y., Ferguson, J. B., Ward, J. V., Fang, H., Pfluger, J. E., Dudis, D. S., Ruan, X., and Wu, Y., 2013. "Measurement of thermal conductivity of pbte nanocrystal coated glass fibers by the 3ω method". Nano Lett., 13, pp. 5006–5012.
[15] Xing, C., Jensen, C., Munro, T., White, B., Ban, H., and Chirtoc, M., 2014. "Accurate thermal property measurement of fine fibers by the 3ω technique". Appl. Therm. Eng., 73, pp. 317–324.
[16] Xing, C., Jensen, C., Munro, T., White, B., Ban, H., and Chirtoc, M., 2014. "Thermal property characterization of fine fibers by the 3ω technique". Appl. Therm. Eng., 71, pp. 589–595.
[17] Munro, T., Xing, C., Ban, H., Copeland, C., Lewis, R., and Glorieux, C. "Thermal property measurement of thin fibers-a direct approach".
[18] Kommandur, S., Mahdavifar, A., Hesketh, P. J., and Yee, S., 2015. "A microbridge heater for low power gas sensing based on the 3ω technique". Sens. and Actuators A, 233, pp. 231–238.
[19] Hou, J., Wang, X., and Guo, J., 2006. "Thermal characterization of micro/nanoscale conductive and non-conductive wires based on optical heating and electrical thermal sensing.". J. Phys. D: Appl. Phys., 39, pp. 3362–3370.
[20] Guo, J., Wang, X., Geohegan, D. B., Eres, G., and Vincent, C., 2008. "Development of pulsed laser-assisted thermal relaxation technique for thermal characterization of microscale wires". J. Appl. Phys., 103, p. 113505.
[21] Guo, J., Wang, X., Geehegan, D. B., and Eres, G., 2008. "Thermal characterization of multi-wall carbon nanotube bundles based on pulsed laser-assisted thermal relaxation". Funct. Mater. Lett., 1, pp. 71–76.
[22] Guo, J., Wang, X., and Wang, T., 2007. "Thermal characterization of microscale conductive and nonconductive wires using transient electrothermal technique". J. Appl. Phys., 101, p. 063537.
[23] Park, B. K., Park, J., and Kim, D., 2010. "Note: Three-omega method to measure thermal properties of subnanoliter liquid samples". Rev. Sci. Instrum., 81, p. 066104.
[24] Lee, S. M., 2009. "Thermal conductivity measurement of fluids using the 3ω method". Rev. Sci. Instrum., 80, p. 024901.
[25] Gao, J., Xie, D., Xiong, Y., and Yue, Y., 2018. "Thermal characterization of microscale heat convection in rare-gas environment by a steady state "hot wire" method". Appl. Phys. Express, 11, p. 066601.
[26] Yang, J., Waltermire, S., Chen, Y., Zinn, A. A., Xu, T., and Li, D., 2010. "Contact thermal resistance between individual multiwall carbon nanotubes". Appl. Phys. Lett., 96, p. 023109.
[27] Guo, L., Wang, J., Lin, Z., Gacek, S., and Wang, X., 2009. "Anisotropic thermal transport in highly ordered tio_2 nanotube arrays". J. Appl. Phys., 106, p. 123526.
[28] Wang, J., Song, B., Gu, M., and Zhang, X., 2010. "Temperature dependence of thermal resistance of a bare joint". Int. J. Heat Mass Trans., 53, pp. 5350–5354.
[29] Wang, J. L., Gu, M., Zhang, X., and Song, Y., 2009. "Thermal conductivity measurement of an individual fibre using a t type probe method". J. Phys. D: Appl. Phys., 42, p. 105502.

[30] Wang, J., Gu, M., Zhang, X., and Wu, G., 2009. "Measurements of thermal effusivity of a fine wire and contact resistance of a junction using a t type probe". Rev. Sci. Instrum., 80, p. 076107.
[31] Bourgeois, O., André, E., Macovei, C., and Chaussy, J., 2006. "Liquid nitrogen to room-temperature thermometry using niobium nitride thin films". Rev. Sci. Instrum., 77, p. 126108.
[32] Carslaw, H., and Jaeger, J., 1959. Conduction of heat in solids. Oxford at Clarendon Press.
[33] Demirel, Y., and Saxena, S. C., 1996. "Heat transfer in rarefied gas at a gas-solid interface". Energy, 21, pp. 99–103.
[34] Kuehn, T., and Goldstein, R., 1976. "Correlating equations for natural convection heat transfer between horizontal circular cylinders". Int. J. Heat Mass Trans., 19(10), pp. 1127–1134.
[35] Maxwell, J. C., 1890. "The scientific papers of james clerk maxwell.".
[36] Kennard, E. H., 1938. Kinetic energy of gases. Mc Graw - Hill book company.
[37] Hadj-Nacer, M., Maharjan, D., Ho, M. T., Stefanov, S. K., Graur, I., and Greiner, M., 2017. "Continuum and kinetic simulations of heat transfer trough rarefied gas in annular and planar geometries in the slip regime". J. Heat Trans., 139, pp. 042002–04010.
[38] Spurgeon, W. A., 2018. Thermal conductivities of some polymers and composites. Technical report, US Army Research Laboratory, Cambridge, MA, Feb. See also URL \\https://www.arl.army.mil/arlreports/2018/ARL-TR-8298.pdf.
[39] Kittel, C., 1949. "Interpretation of the thermal conductivity of glasses". Phys. Rev., 75(6), pp. 972–974.
[40] Babcock, C. L., 1963. "Thermal conductivities of glass between -150^{0}c and 100^{0}c". Glass Technology, 4(4), Augus.
[41] Ratcliffe, E. H., 1961. "Symposium on heat transfer phenomena in glass.". J. Am. Ceram. Soc., 44(7), July.
[42] Ftouni, H., Tainoff, D., Richard, J., Lulla, K., Guidi, J., Collin, E., and Bourgeois, O., 2013. "Specific heat measurement of thin suspended sin membrane from 8 k to 300 k using the 3ω-völklein method". Rev. Sci. Instrum., 84(9), p. 094902.
[43] Ftouni, H., Blanc, C., Tainoff, D., Fefferman, A. D., Defoort, M., Lulla, K. J., Richard, J., Collin, E., and Bourgeois, O., 2015. "Thermal conductivity of silicon nitride membranes is not sensitive to stress". Phys. Rev. B, 92(12), p. 125439.
[44] Fujii, T., Fujii, M., and Honda, T. "Theoretical and experimental studies of the free convection around a long horizontal thin wire in air.". Proceedings of the 7th International Heat Transfer Conference, Munich, Germany, 1982, 2, p. 311.
[45] Jack Hu, X., Jain, A., and K.E., G., 2008. "Investigation of the natural convection boundary condition in microfabricated structures.". International Journal of Thermal Sciences, 47, p. 820.
[46] Wang, H., Liu, J., Zhang, X., Li, T., Zhang, R., , and Wei, F., 2013. "Heat transfer between an individual carbon nanotube and gas environment in a wide knudsen number regime.". Journal of Nanomaterials, 2013, p. 3.
[47] Fujiwara, S., Zhang, X., and Fujii, M., 2001. "Short-hot-wire method for the measurement of total hemispherical emissivity of a fine fibre.". High Temperatures-High pressures, 33, p. 271.
[48] Kim, K., Chung, J., Hwang, G., Kwon, O., and Lee, J., 2011. "Quantitative measurement with scanning thermal microscope by preventing the distortion due to the heat transfer through the air.". ACS Nano, 5, p. 8700.
[49] Shi, L., and Majumdar, A., 2002. "Thermal transport mechanisms at nanoscale point contacts.". J. Heat Transfer, 124, p. 329.
[50] Bresson, B., Brun, C., Buet, X., Chen, Y., Ciccotti, M., Gateau, J., Jasion, G., Petrovich, M., Poletti, F., Richardson, D., Sandoghchi, S., Tessier, G., Tyukodi, B., and Vandembroucq, D., 2017. "Thermal transport mechanisms at nanoscale point contacts.". Phys. Rev. Lett., 119, p. 235501.
[51] Fiorino, A., Thompson, D., Zhu, L., Song, B., Reddy, P., and Meyhofer, E., 2018. "Giant enhancement in radiative heat transfer in sub-30 nm gaps of plane parallel surfaces.". Nano Lett., 18, p. 3711.
[52] Song, B., Thompson, D., Fiorino, A., Ganjeh, Y., Reddy, P., and Meyhofer, E., 2016. "Radiative heat conductances between dielectric and metallic parallel plates with nanoscale gaps.". Nature Nanotech., 11, p. 509.